A clinico-molecular predictor identifies follicular lymphoma patients at risk of early transformation after first-line immunotherapy

Chloé B. Steen,[1,2] Ellen Leich,[3] June H. Myklebust,[2,4] Sandra Lockmer,[5] Jillian F. Wise,[2,4] Björn E. Wahlin,[5] Bjørn Østenstad,[6] Knut Liestøl,[1,7] Eva Kimby,[5] Andreas Rosenwald,[3] Erlend B. Smeland,[2,4] Harald Holte,[4,6] Ole Christian Lingjærde[1,4,8,] and Marianne Brodtkorb[2,4,6,*]*

**OCL and MB contributed equally to this study.*

[1]*Department of Informatics, University of Oslo, Oslo, Norway;* [2]*Department of Cancer Immunology, Institute for Cancer Research, Oslo University Hospital, Oslo, Norway;* [3]*Institute of Pathology, University of Würzburg and Comprehensive Cancer Centre Mainfranken, Germany;* [4]*KG Jebsen Centre for B-Cell Malignancies, Institute for Clinical Medicine, University of Oslo, Oslo, Norway;* [5]*Division of Haematology, Department of Medicine at Huddinge, Karolinska Institute and University Hospital, Stockholm, Sweden;* [6]*Department of Oncology, Oslo University Hospital, Oslo, Norway;* [7]*Institute for Cancer Genetics and Informatics, Oslo University Hospital, Oslo, Norway; and* [8]*Department of Cancer Genetics, Institute for Cancer Research, Oslo University Hospital, Oslo, Norway*

Correspondence: OLE C. LINGJÆRDE - ole@ifi.uio.no

MARIANNE BRODTKORB - meide@ous-hf.no

doi:10.3324/haematol.2018.209080

SUPPLEMENTAL MATERIAL

For the paper:

Steen CB, Leich E, Myklebust JH, Lockmer S, Wise JF, Wahlin B, Østenstad B, Liestøl K, Kimby E, Rosenwald A, Smeland EB, Holte H, Lingjærde OC and Brodtkorb M. A clinico-molecular predictor identifies follicular lymphoma patients at risk of early transformation after first-line immunotherapy

Contents:

SUPPLEMENTAL METHODS

Diagnostic FL biopsies were included from 82 FL patients receiving first-line rituximab treatment with or without interferon-α in two prospective randomized open-label trials[1-3]. FL grade 3B cases were not included. All these samples were obtained prior to the start of the chemotherapy-free regimen. Treatment given at relapse or progression varied. Nine patients had an additional biopsy obtained at a later time point showing FL, and eight of these were obtained before new treatment for relapse or progression was administered. For one patient, an additional lymph node biopsy obtained six years prior to the diagnosis of FL revised by an expert hematopathologist revealed previously undiagnosed FL and was included in the study. Thus, a total of 92 FL biopsies were included, referred to as the rituximab cohort. See Supplemental Figure S1 for an overview of time related events in this cohort. The long-term follow-up of these two chemotherapy-free trials was recently published,[3] and demonstrated that overall survival in these cohorts is at least as good as that observed in modern immunochemotherapy trials.[3-6]

Gene expression and DNA copy number profiles were generated from all 92 samples. In addition, 75 FL biopsies from 44 patients treated with traditional chemotherapy prior to the introduction of rituximab, referred to as the chemotherapy cohort, were used for comparison of molecular features in FL biopsies across treatment cohorts, as well as with *de novo* DLBCL. Clinical data, gene expression data and copy number profiles from this previously published chemotherapy cohort are described elsewhere.[7,8] The study was approved by the Regional Committee for Research Ethics (protocol number S-05209 and 2014/172) and was conducted in accordance with the Declaration of Helsinki. Informed consent was given by all patients upon inclusion in the clinical trials and repeated for all patients alive at last follow-up to allow collection of clinical long-term data.

DNA for copy number analysis and mRNA for gene expression analysis were isolated from fresh frozen sections using the AllPrep mini kit from Qiagen (Qiagen, Hilden, Germany) according to the manufacturer's instructions, and analysed on the Affymetrix SNP6.0 (copy number) and HG U133 plus 2.0 (gene expression) platforms. Raw intensity data (CEL) files were generated by the command console, and quality control of the SNP6.0 and HG U133 plus 2.0 data was performed using the Genotyping and Expression Console software from Affymetrix.

Integration of copy number and gene expression data

The gene expression CEL files were normalized by Robust Multi-array Average (RMA) using Affy R-package version 1.52.[9] Probes matching the same genes were collapsed by using the average signal. The resulting gene expression file was median-centred across patients. We annotated and integrated copy number and gene expression data following the procedure described in Brodtkorb et al.[8] Copy number profiles were obtained by running the SNP Array 6.0 CEL files through the first step of the PennCNV-Affy pipeline which resulted in logR values for all SNP and CN probes and BAF (B-allele frequency) values for all SNP probes. The data were corrected for GC-content. Piecewise Constant Fitting (PCF) values were calculated from the resulting logR file using the R-package copynumber[10] with parameters kmin=3 and penalty=80. Allele-specific copy number states were estimated from logR and BAF values using ASCAT.[11] Copy number states larger than two were considered as gains, and copy number states below two were considered as losses. For calculation of cis-correlation, real-valued copy number values found by PCF were used. These reflect the actual mixture of tumor cells and infiltrating non-tumor cells in a sample and are more directly comparable to gene expression values than ASCAT estimates which are designed to reflect

only the tumor cell component of a sample. See Supplemental table 1 and Supplemental Figures S3-4 for results for both treatment cohorts.

Gene scores

A total of 14 gene signatures were considered, each named after a particular regulator gene in the NF-κB signaling network (see Supplemental Table 2). For each NF-κB regulator, the genes in the signature represent the subset of NF-κB target genes highly correlated to the respective regulator (see reference 8 and Supplemental Figure S2 for details). For a given biopsy, the average expression across all genes in a signature constitutes an estimator of the expression for the corresponding regulator gene. Under mild assumptions, this estimator has lower variance than the expression of the regulator gene itself due to the averaging over many similar entities. While the estimator may be slightly biased due to the averaging of genes not following the exact same distribution, it represents a stable low-variance estimate of the expression of the regulator gene and is suitable as a biomarker.

As candidate markers for transformation, we considered six gene signatures previously linked to transformation risk in the pre-rituximab era.[8] For completeness, we included in the preliminary analyses all 14 gene expression signatures involving downstream targets of the NF-κB pathway described in Brodtkorb et al.; see Supplemental Table 2. Raw gene expression scores were calculated as the average log2-expression across all genes in a given signature after median centring and scaling to unit variance the log2-expression of each gene. Score values were found by thresholding raw scores on their median value, with 0 for raw score below median and 1 for raw score above median. FLIPI groups were defined as described by Solal-Celigny et al.[12] Association to transformation was assessed with Student's t-test and Fisher's exact test. Cox proportional hazards regression was used to relate time to transformation and time to new treatment to covariates. Statistical analyses were performed in R (version 3.3.2) and Bioconductor (version 3.4).

Assessing stability and robustness of gene expression scores across patient cohorts

Cis-correlations were calculated using Pearson's correlation coefficient between PCF-segmented[10] log2-transformed copy number values and log2-transformed gene expression values. For each gene expression score, a score shift **Δ** was calculated by subtracting the average score in biopsies from patients experiencing transformation and the average score in biopsies from patients not experiencing transformation. The score shift quantifies the effect on the score values of being a biopsy from a patient with subsequent transformation. Effect sizes in the rituximab cohort and the chemotherapy cohort were compared visually by scatter plot and statistically by linear regression and Pearson's correlation coefficient.

Modelling transformation, time to transformation and time to new treatment

The rituximab cohort was used to model time to transformation and time to new treatment. The earliest biopsy with high score was used if a patient had more than one biopsy. Kaplan-Meier plots were used to estimate and visualize survival distributions. The log-rank test was used to assess differences in survival between groups. Overall survival was defined as the time from diagnosis to death of any cause. Patients alive at last follow-up were censored. For estimation of time to transformation the starting point was the time of FL diagnosis. Events were defined as transformation to DLBCL determined by biopsy. Patients with no signs of transformation during follow-up were censored. No patients were diagnosed with transformation based solely on clinical criteria during follow-up. For estimation of time to new treatment, the starting point was the time of diagnosis. Events were defined as start of treatment for first relapse/progression after primary rituximab treatment, transformation or

lymphoma-related death. Censored patients were either alive at the end of follow-up without transformation or without having received new treatment, or dead from other causes than lymphoma.

Principal component analysis

Principal component analysis (PCA) was applied to gene expression data for the BTK gene signature and a previously published gene signature separating the ABC and GCB subtypes of DLBCL,[13] using all available FL samples (rituximab cohort and chemotherapy cohort, n=167) and a set of *de novo* DLBCL (n=150) from the Leukemia Lymphoma Molecular Profiling Project (LLMPP). A gene expression matrix was defined with columns representing genes and rows representing samples. Scores for the first two principal components were extracted, reducing each sample to a two-dimensional score vector. To test the null hypothesis that the multivariate mean of the two-dimensional score vectors is identical for biopsies from patients with and without transformation, we applied Hotelling's T-square test. To find the optimal linear separation between score vectors corresponding to patients with and without transformation, we applied linear discriminant analysis (LDA). To assess the strength of the association between the LDA separation and the transformation status (i.e. whether or not a biopsy originated from a patient that later experienced transformation), a two-way classification was performed with transformation status and LDA classification (0/1) as variables. The significance of the association between the two variables was assessed by a permutation test. The expression values were gene centered (by subtraction of the mean) and gene scaled (by division with the standard deviation) separately for the rituximab cohort, the chemotherapy cohort and the LLMPP samples. For the first two cohorts, all samples in the respective cohort were used to calculate the mean and the standard deviation used for the centering and the scaling. The FL LLMPP data (n=191) were used to calculate the mean and the standard deviation used for the centering and the scaling of the DLBCL LLMPP data. This ensured compatible centering of the DLBCL samples relative to the samples in the rituximab cohort and the chemotherapy cohort. The FL LLMPP data set were not used for any other purpose in our analysis. To calculate a confidence region for a PCA centroid, we calculated the covariance matrix of the two principal component scores for all samples defining the centroid. To obtain the covariance for the centroid itself, the matrix was divided by the number of samples. A confidence region was plotted using the R-package ellipse. To formally assess the separation of the two centroids, a Hotelling's T-square test was used. See Supplemental Figure 8 for results.

Permutation test

To adjust for the fact that even a random labelling of the FL samples (with vs. without transformation) may result in an LDA separation with small P-value, we performed a permutation test with 1000 permutations of the transformation labelling. For each permutation, a two-way classification was performed as described above and a P-value calculated with a Fisher's exact test. The observed P-value P_{obs} was compared to the 1000 permutation P-values P^*_1, …, P^*_{1000} and the quantile corresponding to P_{obs} was reported as the final LDA P-value. See Supplemental Table 2 for results.

Data availability

Gene expression and SNP6.0 data for the rituximab cohort are deposited at the European Genome-phenome Archive (EGA; http://www.ebi.ac.uk/ega/), which is hosted at the EBI, under accession number EGAS00001002566. The gene expression data for the chemotherapy cohort were available in house and are published online (Accession number GSE53820). The

LLMPP data have been described in previous publications.[14,15] They were accessed online (https://llmpp.nih.gov/).

Code availability

Complete R source code for the analyses performed in this paper will be made available from the website http://heim.ifi.uio.no/bioinf/Projects/.

SUPPLEMENTAL FIGURES

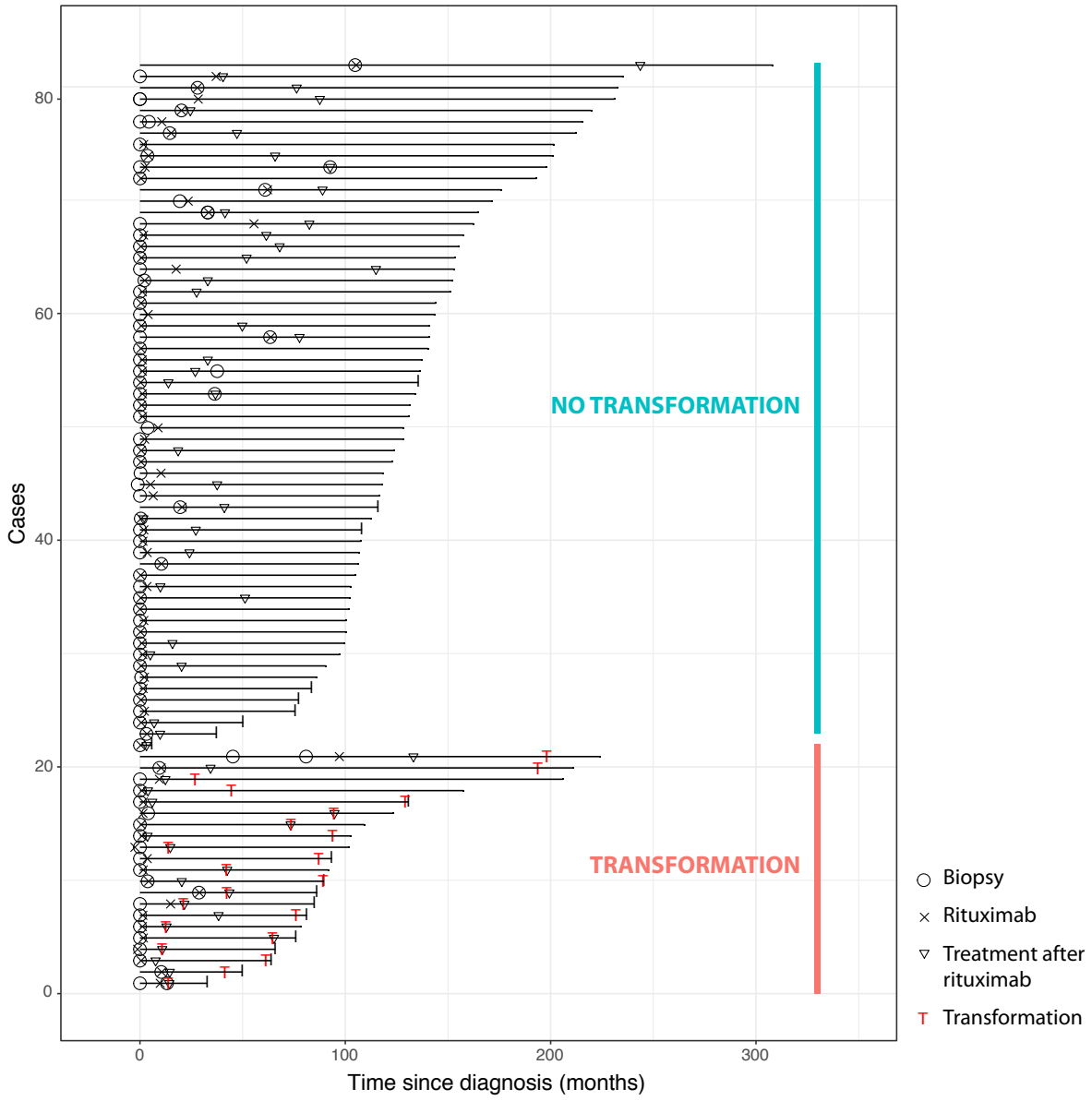

Supplemental Figure S1. Follow-up of FL patients in the rituximab cohort. Each horizontal line represents a patient, with the length of the line representing the time in months between diagnosis and last date of follow up. Patients are divided in two groups according to transformation status (FL patients without transformation: n=61; FL patients with transformation: n=21). Open circles show the time points at which the examined biopsies were obtained. Crosses represent the time points of initiation of rituximab treatment. Triangles represent the time points at which new treatment was administered for relapse after rituximab. Red T's represent the time points at which transformation was first observed.

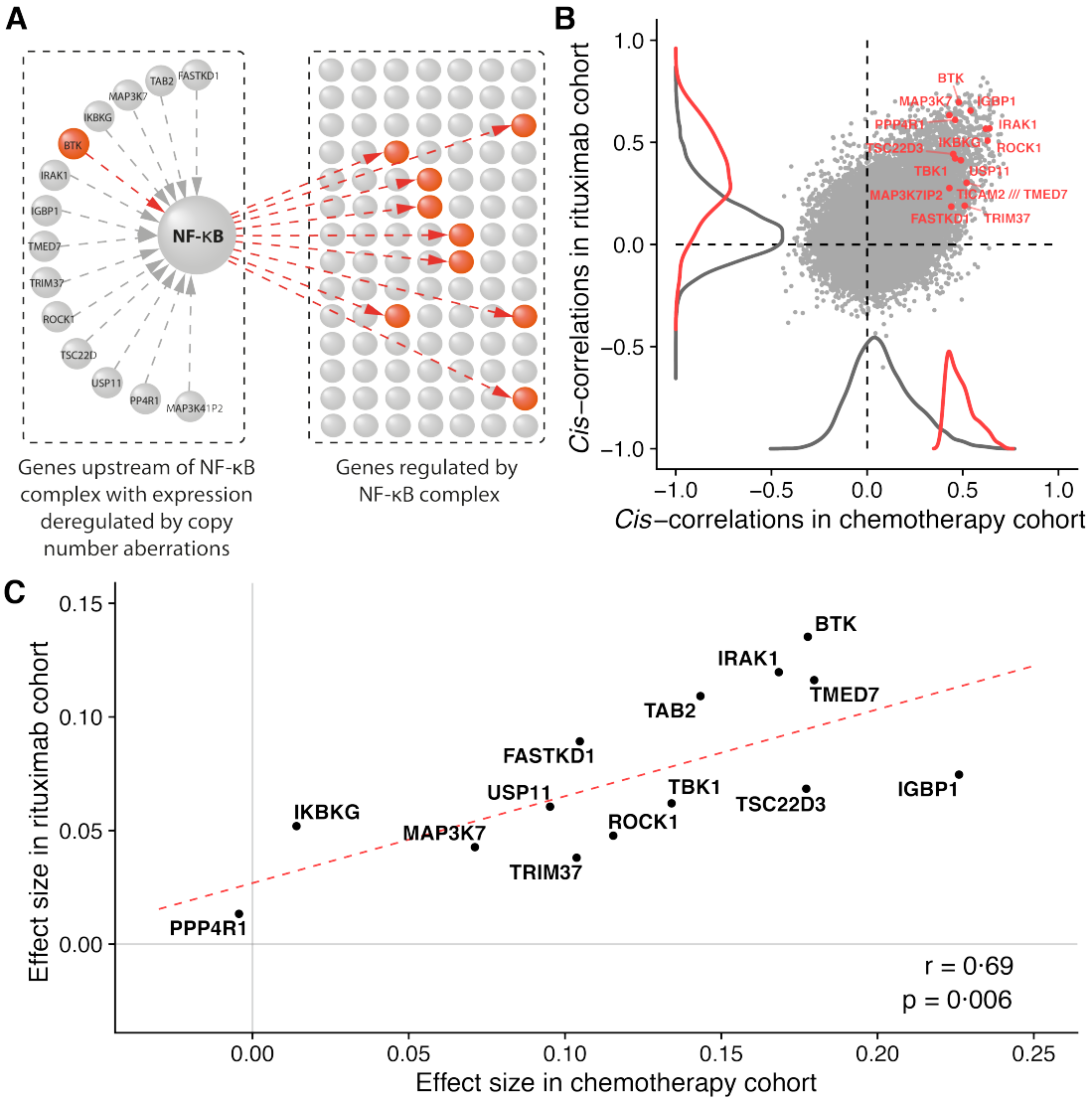

Supplemental Figure S2. The NF-κB pathway deregulation scores. (A) Schematic representation of the 14 copy-number driven genes upstream of NF-κB and their corresponding downstream signatures, as described in Brodtkorb et al.[8] The 14 genes were identified by gene set enrichment analysis of genes with strong association between copy number and gene expression. For each of the 14 genes, a permutation test was applied to identify highly correlated NF-κB target genes. Low-variance expression estimators (scores) for the 14 genes were subsequently derived by averaging over the expression of the selected target genes. (B) Pearson's correlation coefficient between correlations of gene expression and copy number in the chemotherapy cohort (horizontal axis; n=75 biopsies) and the rituximab cohort (vertical axis; n=92 biopsies). Correlation coefficients of the 14 genes described above are shown in red and the remaining genes are shown in grey. The correlation coefficients are given in Supplemental Table 1. (C) Effect size in the chemotherapy (discovery) cohort (horizontal axis) and the rituximab cohort (vertical axis) for the 14 low-variance expression estimators (scores). The effect size reflects the change in mean score when biopsies from patients with and without transformation were compared. The red line represents the linear regression fit to the data points (P=0.006). The Pearson correlation between the effect sizes in the two cohorts is $r = 0.69$. The genes constituting each of the NF-κB target gene signatures are listed in Supplemental Table 2.

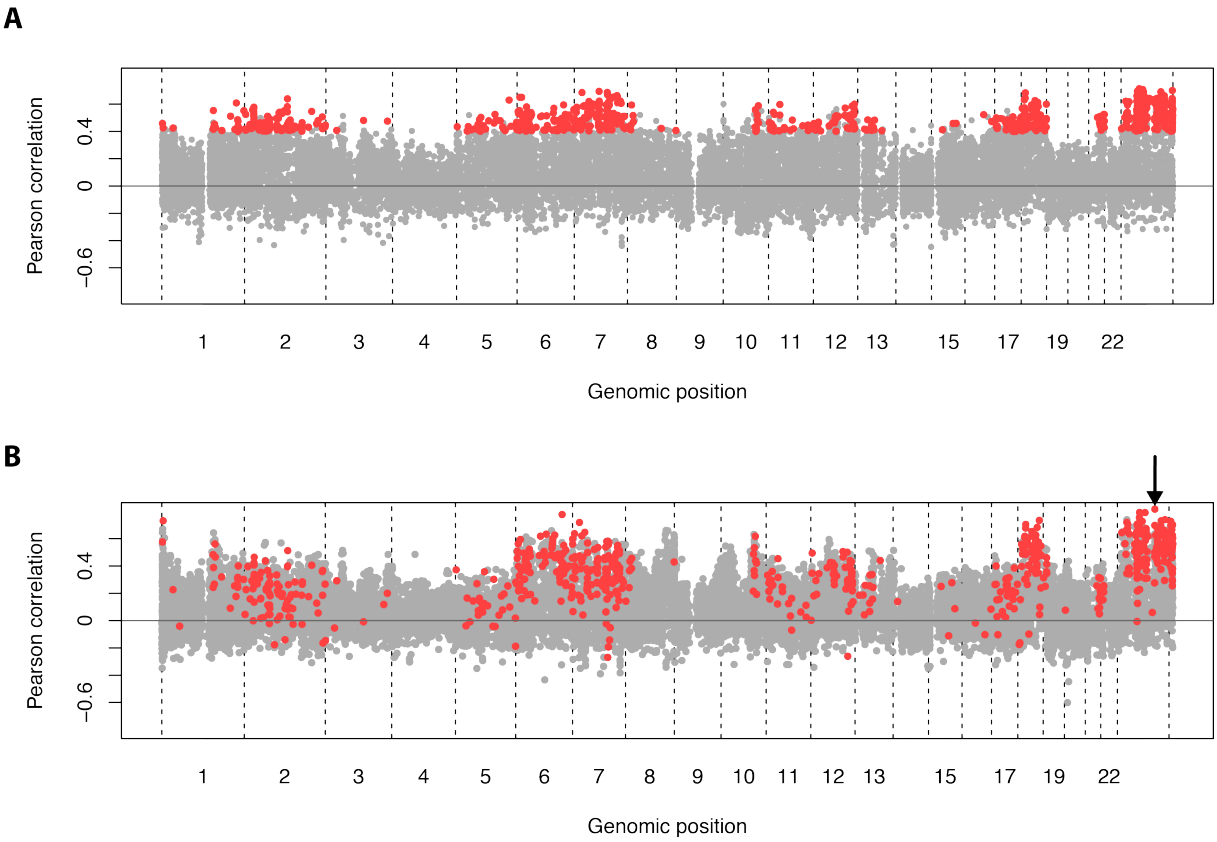

Supplemental Figure S3. Association between DNA copy number and gene expression. Each point represents a gene, with the horizontal axis representing the chromosomal position of the gene and the vertical axis representing the Pearson correlation between gene expression and copy number. (A) Pearson correlations in the chemotherapy cohort (n=75 biopsies). Genes with Pearson correlation above 0.4 and a significant difference in gene expression when comparing cases with no copy number change and cases with loss or gain are shown in red (n=698) from Brodtkorb et al.[8]. (B) Pearson correlations in the rituximab cohort (n=92 biopsies). Shown in red are the same 698 genes as shown in red in (A). The black arrow shows the correlation coefficient for the gene BTK located in a region of frequent copy number gain on chromosome X.

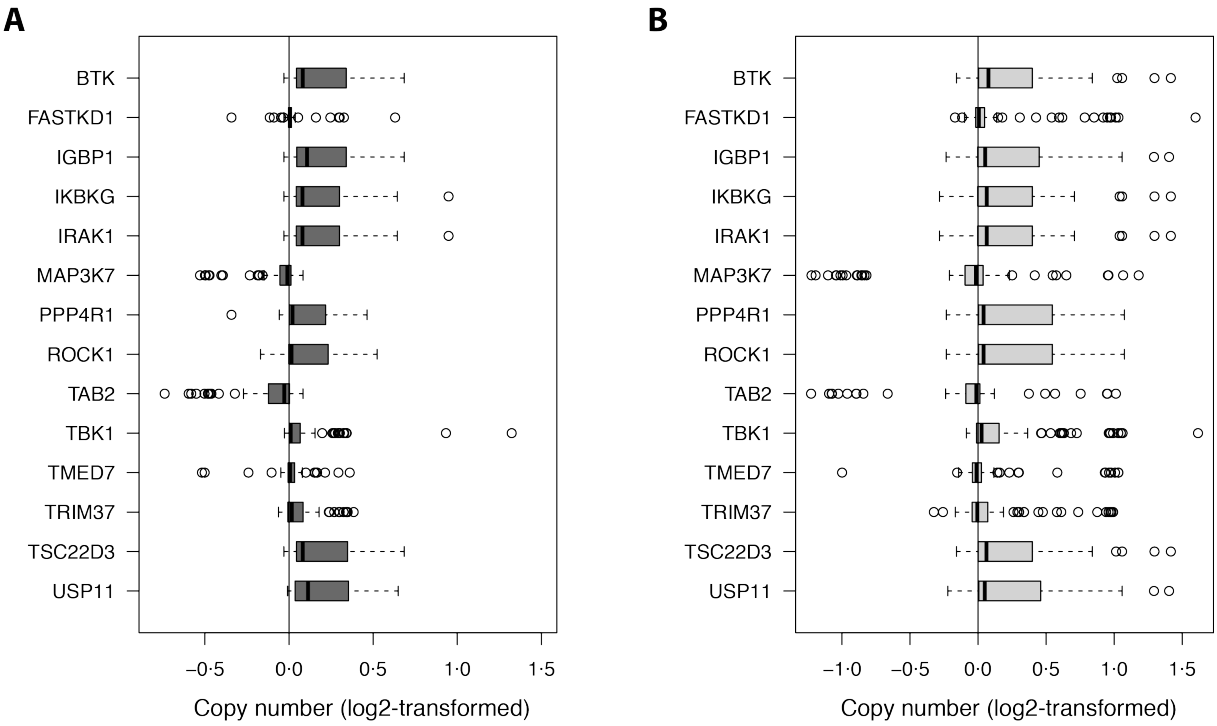

Supplemental Figure S4. Distribution of DNA copy number in the 14 upstream regulators of NF-κB. The figure shows the distribution of DNA copy number in each of the two cohorts for the 14 upstream regulators of NF-κB shown in Supplementary Figure 2A. Gene identifiers are shown along the left side of each panel. (A) Distribution of DNA copy number in the chemotherapy cohort (n=75 biopsies). Shown along the horizontal axis are copy number measurements obtained by array CGH and segmented by piecewise constant fitting (PCF) after log2-transformation, as described in Brodtkorb et al.[8]. (B) Distribution of DNA copy number in the rituximab cohort (n=92 biopsies). Shown along the horizontal axis are copy number measurements obtained by SNP6.0 array and processed by the Allele-Specific Copy Number Analysis in Tumours (ASCAT) algorithm (see Supplemental Methods). The values in the rituximab cohort were log2-transformed to be on the same scale as in the chemotherapy cohort.

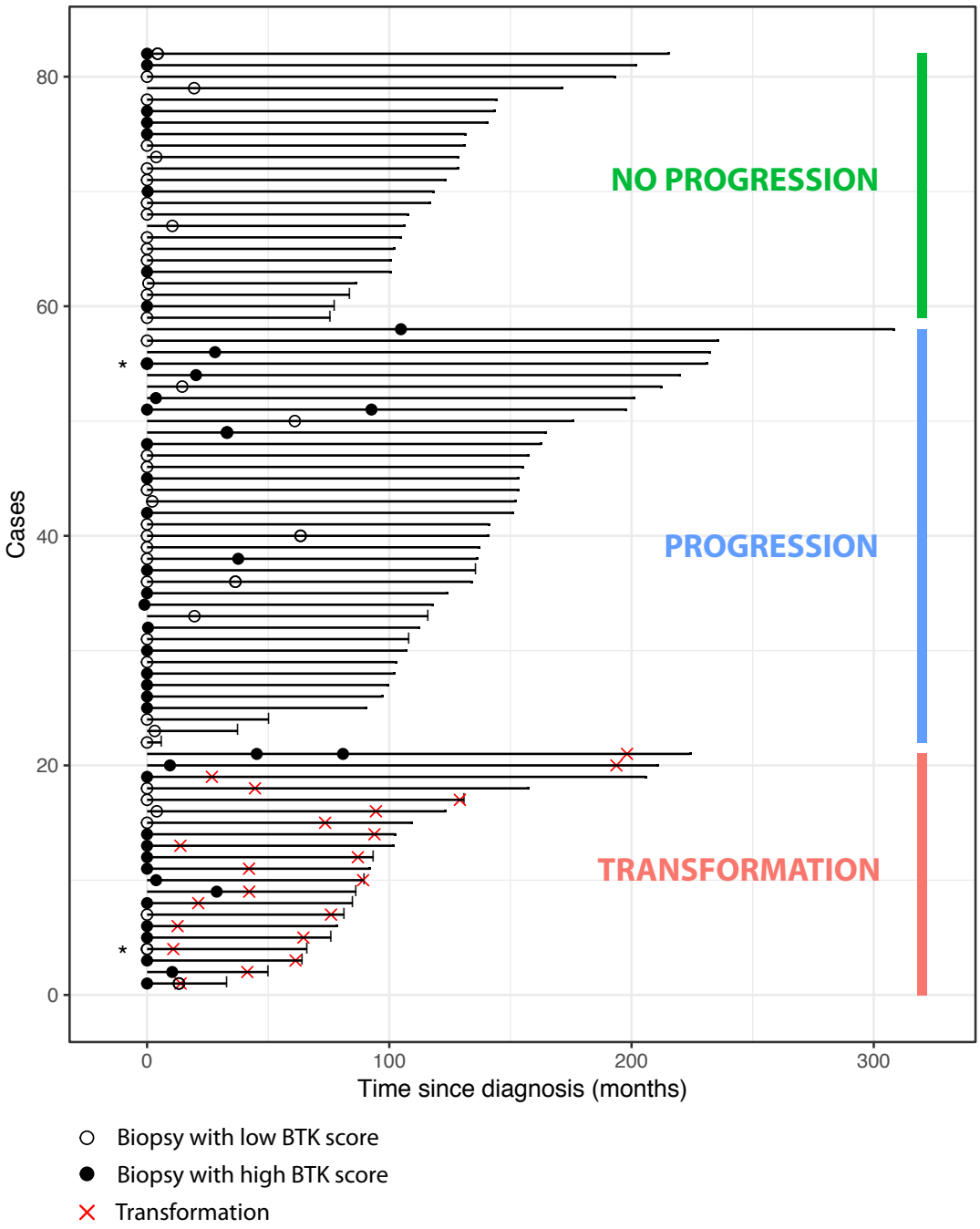

Supplemental Figure S5. Distribution of biopsies with high BTK score in the rituximab cohort. Each horizontal line represents a patient, with the length of the line representing the time in months between diagnosis and last date of follow up. Patients are divided in three groups according to disease outcome following the primary treatment with rituximab +/- interferon-alfa: Patients without progression and no need of new lymphoma treatment (Green, n=24); patients with progression of indolent disease and need of new treatment (Blue, n=37); patients progressing with transformation (Red, n=21). Open circles represent biopsies showing low BTK score (below median). Filled circles represent biopsies showing high BTK score (above median). Crosses represent the time points at which transformation was first observed. *One patient had a biopsy that was obtained six years prior to diagnosis and analyzed retrospectively (case 4), another patient had two biopsies taken at the same time, at different sites (case 55).

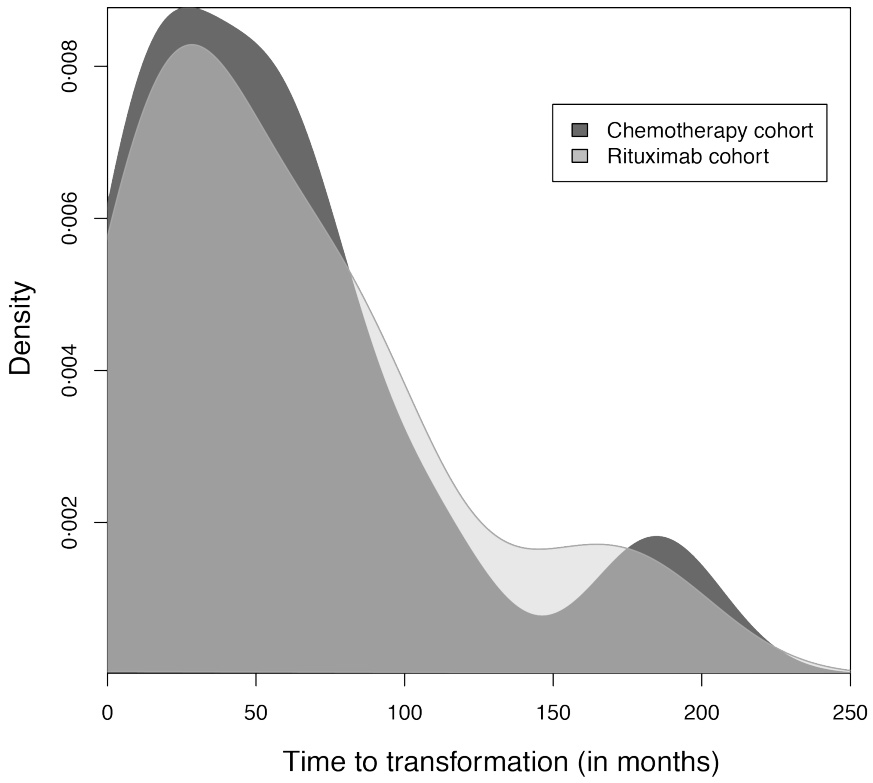

Supplemental Figure S6. Time from detection of high BTK score to diagnosis of transformation. The figure is based on data from the FL biopsies obtained from patients with later transformation that showed a high BTK score (score above median) prior to transformation (n=10 for the chemotherapy cohort and n=15 for the rituximab cohort). The horizontal axis represents the time from the FL biopsy with high BTK score to the time of transformation. The vertical axis represents the probability density.

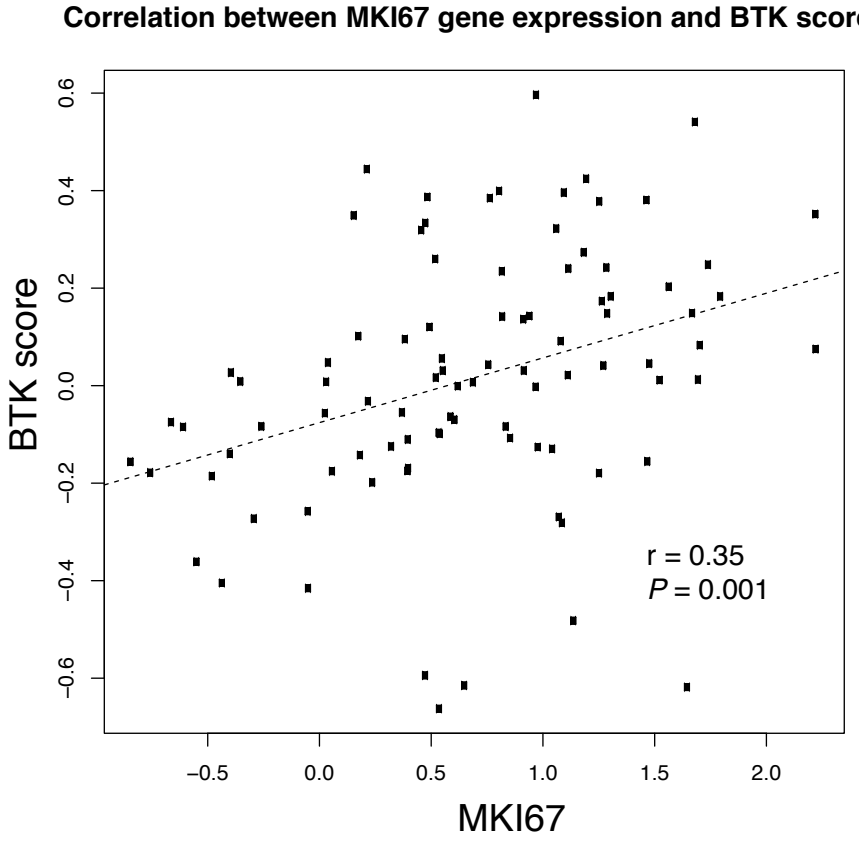

Supplemental Figure S7. Correlation between MKI67 gene expression and BTK score. Each dot represents a biopsy (n=92). The gene expression values are log2 normalized and median-centered. The dotted line represents the linear regression fit to the data points (P=0.001). The Pearson correlation between the MKI67 gene expression and the BTK score is $r = 0.35$.

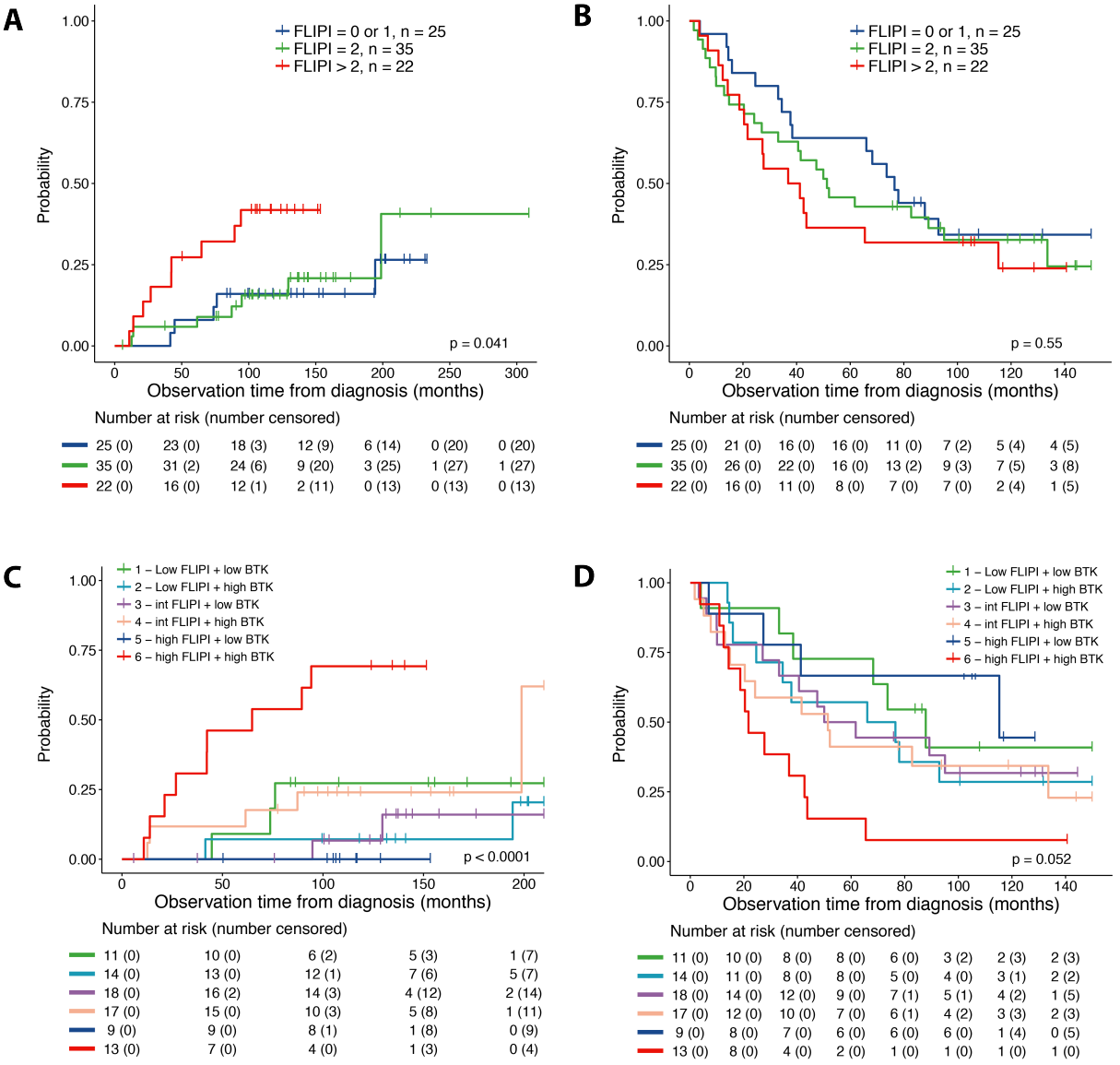

Supplemental Figure S8. Patient stratification with FLIPI and BTK-FLIPI. The analysis was performed on patients in the rituximab cohort (n=82). (A) Kaplan-Meier plot of time to transformation in FLIPI risk groups: Low risk (0 or 1, blue, n=25); intermediate risk (2, green, n=35) and high risk (3 or higher, red, n=22) (Logrank test: P=0.0041; n=82 patients). (B) Kaplan-Meier plot of time to new treatment in FLIPI risk groups: Low risk (0 or 1, blue, n=25), intermediate risk (2, green, n=35) and high risk (3 or higher, red, n=22) (Logrank test: P=0.55; n=82 patients). (C) Time to transformation according to the six different combinations of the BTK-FLIPI score (Logrank test: P<0.0001; n=82 patients). (D) Time to new treatment according to the six different combinations of the BTK-FLIPI score (Logrank test: P=0.052; n=82 patients).

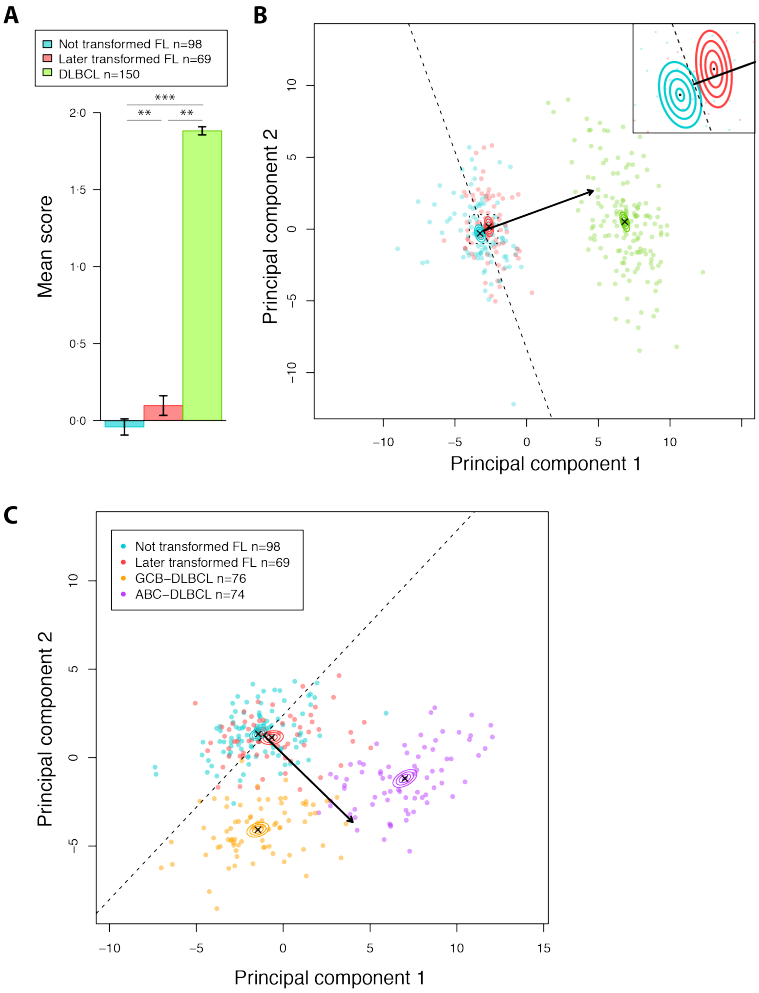

Supplemental Figure S9. Shift in BTK signature in FL with transformation. (A) Mean BTK score in FL biopsies from patient without transformation (cyan; n=98), FL biopsies from patients with subsequent transformation (red; n=69) and *de novo* DLBCL biopsies (green; n=150). The black bars represent the standard error of the mean. The symbols (**) and (***) indicate a P-value smaller than 0.01 and 0.001, respectively. (B) The first two principal components for the BTK gene signature, based on the same biopsies as in (A). Each point represents a biopsy. The dashed line represents the linear discriminant giving the best separation between FL biopsies from patients with and without transformation. The arrow is orthogonal to the separation line and represents the principal component gradient between FL biopsies from patients with and without transformation. Ellipses represent (from largest to smallest ellipse) 95%, 80%, 50% and 10% confidence regions around the centroids. The upper right corner is a scaled-up view of the centroids (shown as a stapled box in the main plot). (C) The first two principal components of all FL biopsies (n=167) and 150 *de novo* DLBCL biopsies from LLMPP, for a previously published gene list in Davies et al. (2007). Each point represents a biopsy. The dashed line represents the linear discriminant giving the best separation between FL biopsies from patients with and without transformation. The arrow is orthogonal to the separation line and represents the principal component gradient between FL biopsies from patients with and without transformation. Ellipses represent (from largest to smallest ellipse) 95%, 80%, 50% and 10% confidence regions around the centroids. Cyan: FL biopsies from patients without transformation (n=98); red: FL biopsies from patients with transformation (n=70); orange: GCB-DLBCL biopsies (n=76); magenta: ABC-DLBCL biopsies (n=74).

SUPPLEMENTAL TABLES

Supplemental Table S1. Pearson correlation between DNA copy number and gene expression for the 14 upstream regulators of NF-κB.

Gene	Chemotherapy cohort	Rituximab cohort
BTK	0.48	0.70
FASTKD1	0.44	0.19
IGBP1	0.54	0.66
IKBKG	0.62	0.57
IRAK1	0.64	0.57
MAP3K7	0.43	0.63
MAP3K7IP2	0.43	0.28
PPP4R1	0.46	0.61
ROCK1	0.63	0.51
TBK1	0.46	0.42
TMED7	0.52	0.30
TRIM37	0.51	0.19
TSC22D3	0.45	0.44
USP11	0.49	0.41

Supplemental Table S2. Genes included in the 14 gene signatures derived from NF-κB target genes, from Brodtkorb et al[8].

Gene	Genes included in the gene signature
BTK	*BAX, C10orf10, CCR7, CCT3, CD22, CDGAP, CTTN, EMR1, FCRL2, FRMD4A, IER3, LAMP3, LRRC32, MRPS10, MRTO4, MYO7A, NOB1, PA2G4, PLK3, PMP22, PTGES2, PTGES3, RGL1, SFRS6, SIRPB1, SNRPB, SNRPD3, SPECC1, SSTR2, TMSB4X /// TMSL3, TNFAIP3, TNFSF13B, TOR3A, TRAF1, USP18, ZBED1, ZNF530*
FASTKD1	*ANP32A /// ANP32C, BIRC3, CCT3, DENND4A, DRAM, ECE1, EPSTI1, FAM177A1, FLJ22374, FLVCR1, GNG10, GRPEL1, IFI44L, IFIH1, IFIT3, JMJD8, LACTB, LTB4R, LYPLA2, LYSMD2, MAP3K8, MRPS10, MYC, NAMPT, NFE2L3, NP, PLAGL1, PLK3, POU5F1 /// POU5F1, PTGES2, PTGES3, PVRL1, SEMA7A, SGK1, SLC39A3, SNRPD3, SPNS2, TCF20, TGFB3, TGM1, TMPRSS6, TNFSF13B, ZNF283, ZNF787*
IGBP1	*ADAM8, CCR7, CCT3, ECE1, FRMD4A, GRPEL1, ICAM1, IER3, IL6, LAMP3, LRRC32, MAP3K8, MRPS10, MVK, MYO7A, NOSIP, PA2G4, PIK3CD, PTGES3, RASGRP1, RPS6KB2, SLC39A3, SNRPB, SNRPD3, SOCS3, SPECC1, STAT3, TNFAIP2, TNFAIP3, TOR3A, VPS53, ZBED1, ZMIZ2,*
IKBKG	*ANP32A /// ANP32C, CD36, ECE1, FAM177A1, FAM65B, FRMD4A, GNG10, IFI44L, IFIH1, IFIT3, JMJD8, LYPLA2, MARCKS, MRPS10, MVK, NAMPT, NCF2, NFE2L3, NR1D2, PLAGL1, PLK3, PTGES2, PVRL1, RFTN1, RGL1, SAMSN1, SLC39A3, SRF, STK35, TCEB3, TCOF1, TGM1, TNFAIP3, TNFRSF21, TNFSF13B, URM1, USP18, ZBED1, ZMIZ2, ZNF283, ZNF507, ZNF787*
IRAK1	*APBB2, BATF, BCL2L1, CTTN, ECE1, ENO1, EPHB1, FAM65B, FEZ1, GLDC, IFI44L, IRF4, KCNN4, LPCAT3, MVK, NCF2, NDE1, NFKB1, NFKB2, PA2G4, PIK3CD, RGL1, RPL7L1, SAMSN1, SIRPA, SLC38A5, SLC39A3, SNRPB, SRF, SSTR2, TCOF1, USP18, ZBED1, ZNF507*
MAP3K7	*ABTB2, ADAD2, ANP32A /// ANP32C, B3GNT7, BAX, C17orf51, C6orf58, CCND2, CCT3, CSNK2A1, CTTN, CYP2J2, DENND4A, EIF5A, EPSTI1, FLJ22374, FLJ38359, FLVCR1, FUS, ICAM1, IFIH1, IL4I1 /// NUP62, IRF4, JMJD8, LPCAT3, LRG1, LRRC32, LTB, MARCKS, MREG, MRPS10, MYC, NAMPT, NR1D2, PIK3CD, PLAGL1, PLK3, POU5F1 /// POU5F1, PSMD11, PTGES2, PTGES3, PVRL1, SAMSN1, SEMA7A, SH2D5, SLC39A3, SSTR2, STAT3, STX11, TAPBP, TCF20, TGFB3, TGM1, TMPRSS6, URM1, VASP, ZBED1*
PPP4R1	*APBB2, BCL2A1, C7orf50, CD40, CSRP2, DGAT2, EPHB1, FAM65B, FCRL2, FEZ1, GADD45B, IL12A, IRF4, LAMP3, LMO2, LOC283663, LTB, MAP3K8, MOBKL2C, NCF2, POLR3A, PSMD11, RAB7L1, SSTR2, TJP2, TNF, ZMIZ2, ZNF530*
ROCK1	*APBB2, BASP1, BATF3, C7orf50, CCDC28B, CCND2, CD22, CSNK2A1, CSRP2, CYB561, DENND4A, DGAT2, DRAM, ECE1, EMR1, FEZ1, FLJ22374, FLVCR1, FUS, GADD45B, GNG10, IRF4, LPCAT3, MARCKS, MOBKL2C, MYO7A, NCF2, NDE1, NFKB2, NOSIP, PES1, PIK3CD, POLR3A, PSMD11, RASGRP1, RFTN1, RPL7L1, RPS6KB2, SFRS6, SSTR2, STK35, TAPBP, TCF20, TCOF1, TNFSF13B, TOR3A, TTC39C, USP18, VPS53, ZNF507, ZNF530*
TAB2	*B3GNT7, CCDC28B, CCND2, CCR7, CDGAP, CSNK2A1, CTTN, DENND4A, EMR1, EPSTI1, FLJ22374, GLDC, ICAM1, IFIH1, IRF1, IRF4, LOC440934, LPCAT3, LTB, MREG, MYC, MYO7A, NAGPA, NFKB1, NFKB2, PIK3CD, PLAGL1, PRMT1, PSMD11, PSME1, PTGER4, PVRL1, RASGRP1, SAMSN1, SIRPA, SLC39A3, SOCS3, SSTR2, STAT3, STAT5A, STX11, TAPBP, TGM1, TLR2, TMPRSS6, TNF, TNFAIP3, TNFSF13B, TRAF1, URM1, VAV1, ZNF787*
TBK1	*ANP32A /// ANP32C, BCL2A1, BCL2L1, CCT3, CD80, CTTN, FAM177A1, FLVCR1, GRPEL1, LAT2, MYO7A, PLK3, POU5F1 /// POU5F1, PTGES3, RGS16, SAMSN1, SGK1, TCF20, VASP, VPS53*
TMED7	*ADAD2, ANP32A /// ANP32C, B3GNT7, BATF, BATF3, BCL2A1, BCL2L1, CCND2, CCT3, CD44, CD80, CDGAP, CYB561, CYP2J2, DENND4A, DGAT2, DRAM, DUSP2, EBI3, EMR1, ENO1, EPSTI1, FAM177A1, FCRL2, FLJ22374, FLJ38359, FLVCR1, GLDC, GNG10, GRPEL1, HCK, ICAM1, IFI35, IFI44L, IFIH1, IFIT3, IL10, IRF1, JMJD8, LACTB, LMO2, LOC283663, LPCAT3, LTB, LTB4R, LYSMD2, MAP3K8, MIRHG1, MREG, MRPS10, NAMPT, NCF2, NFE2L3, NFKB2, NFKBIA, NP, PA2G4, PES1, PLAGL1, PLK3, POU5F1 /// POU5F1, PRMT1, PSME1, PTGER4, PTGES3, PVRL1, RAB7L1, RASSF4, RGL1, RPL7L1, SAMSN1, SEMA7A, SGK1, SH2D5, SIRPA, SIRPB1, SPECC1, STAT3, STAT5A, STX11, TAGLN2, TAPBP, TCEB3, TCF20, TCOF1, TGM1, TLR2, TMEM109, TMPRSS6, TNFAIP3, TNFSF13B, TOR3A, TTC39C, USP18, VASP, VPS53, ZBED1, ZMIZ2, ZNF787*
TRIM37	*ABTB2, ADAM8, ANP32A /// ANP32C, BATF, BBC3, C7orf50, CCT3, CD40, CSNK2A1, DENND4A, ECE1, FAM177A1, FCRL2, FLJ22374, FLVCR1, FOXJ1, GADD45B, GRPEL1, ICAM1, IER3, IFIH1, JMJD8, LOC149478, LPCAT3, LRG1, LRRC32, LTB, MOBKL2C, MRPS10, NINJ1, NR1D2, PLAGL1, PLK3, POLR3A, POU5F1 /// POU5F1, PSMD11, PTGES2, PVRL1, RASGRP1, SEMA7A, SOCS3, SSTR2, TCF20, TGFB3, TGM1, TMPRSS6, TNFAIP2, UNC119, ZMIZ2, ZNF283, ZNF507, ZNF787*
TSC22D3	*BCL2L1, C17orf51, FOXJ1, GRPEL1, IL6, NAGPA, NOSIP, NR1D2, PA2G4, POU5F1 /// POU5F1, PTGES3, RPS6KB2, TAGLN2, TAPBP, TMEM109, TOR3A, ZBED1*
USP11	*ABTB2, BASP1, BATF3, BCL2A1, BCL2L1, C17orf51, C7orf50, CCT3, CD40, CSNK2A1, CSRP2, CTTN, DGAT2, DRAM, ENO1, EPHB1, FCRL2, FEZ1, FLVCR1, FUS, GNG10, KCNN4, LAMP3, LMO2, LPCAT3, LYPLA2, LYSMD2, MAP3K8, MOBKL2C, NCF2, NDE1, NFKB1, NFKB2, NP, PIK3CD, POLR3A, PSMD11, RAB7L1, RFTN1, RGL1, SAMSN1, SRF, STK35, TAPBP, TCOF1, TNFAIP6, TNFSF13B, URM1, USP18, VPS53, ZBED1, ZNF283*

Supplemental Table S3. Association of genes scores with transformation. The association of the 14 NF-κB gene scores with transformation was assessed with a Student's t-test.

Gene	P-value (Student's t-test)
BTK	0.039
FASTKD1	0.043
IGBP1	0.291
IKBKG	0.32
IRAK1	0.147
MAP3K7	0.516
PPP4R1	0.822
ROCK1	0.441
MAP3K7IP2	0.228
TBK1	0.357
TMED7	0.127
TRIM37	0.457
TSC22D3	0.41
USP11	0.362

Supplemental Table S4. PCA separation of FL with and without subsequent transformation. The separation between FL with and without transformation was assessed by two different statistical tests; the Hotelling's t-test and a permutation test.

Gene	P-value (Hotelling's t-test)	P-value (permutation test)
BTK	0.003	0.004
FASTKD1	0.113	0.260
IGBP1	0.003	0.219
IKBKG	0.555	0.178
IRAK1	0.018	0.148
MAP3K7	0.052	0.284
PPP4R1	0.441	0.041
ROCK1	0.114	0.024
MAP3K7IP2	0.037	0.017
TBK1	0.027	0.028
TMED7	0.015	0.016
TRIM37	0.009	0.090
TSC22D3	0.060	0.294
USP11	0.196	0.017

REFERENCES

1. Kimby E, Jurlander J, Geisler C, et al. Long-term molecular remissions in patients with indolent lymphoma treated with rituximab as a single agent or in combination with interferon alpha-2a: a randomized phase II study from the Nordic Lymphoma Group. *Leuk Lymphoma*. 2008;49(1):102-112.
2. Kimby E, Østenstad B, Brown P, et al. Two courses of four weekly infusions of rituximab with or without interferon-alpha2a: final results from a randomized phase III study in symptomatic indolent B-cell lymphomas. *Leuk Lymphoma*. 2015;56(9):2598-2607.
3. Lockmer S, Østenstad B, Hagberg H, et al. Chemotherapy-Free Initial Treatment of Advanced Indolent Lymphoma Has Durable Effect With Low Toxicity: Results From Two Nordic Lymphoma Group Trials With More Than 10 Years of Follow-Up. *J Clin Oncol*. 2018:JCO1800262.
4. Luminari S, Ferrari A, Manni M, et al. Long-Term Results of the FOLL05 Trial Comparing R-CVP Versus R-CHOP Versus R-FM for the Initial Treatment of Patients With Advanced-Stage Symptomatic Follicular Lymphoma. *J Clin Oncol*. 2018;36(7):689-696.
5. Pastore A, Jurinovic V, Kridel R, et al. Integration of gene mutations in risk prognostication for patients receiving first-line immunochemotherapy for follicular lymphoma: a retrospective analysis of a prospective clinical trial and validation in a population-based registry. *Lancet Oncol*. 2015;16(9):1111-1122.
6. Salles G, Seymour JF, Offner F, et al. Rituximab maintenance for 2 years in patients with high tumour burden follicular lymphoma responding to rituximab plus chemotherapy (PRIMA): a phase 3, randomised controlled trial. *Lancet*. 2011;377(9759):42-51.
7. Eide MB, Liestøl K, Lingjærde OC, et al. Genomic alterations reveal potential for higher grade transformation in follicular lymphoma and confirm parallel evolution of tumor cell clones. *Blood*. 2010;116(9):1489-1497.
8. Brodtkorb M, Lingjærde OC, Huse K, et al. Whole-genome integrative analysis reveals expression signatures predicting transformation in follicular lymphoma. *Blood*. 2014;123(7):1051-1054.
9. Gautier L, Cope L, Bolstad BM, Irizarry RA. affy--analysis of Affymetrix GeneChip data at the probe level. *Bioinformatics*. 2004;20(3):307-315.
10. Nilsen G, Liestøl K, Van Loo P, et al. Copynumber: Efficient algorithms for single- and multi-track copy number segmentation. *BMC Genomics*. 2012;13:591.
11. Van Loo P, Nordgard SH, Lingjærde OC, et al. Allele-specific copy number analysis of tumors. *Proc Natl Acad Sci U S A*. 2010;107(39):16910-16915.
12. Solal-Celigny P, Roy P, Colombat P, et al. Follicular lymphoma international prognostic index. *Blood*. 2004;104(5):1258-1265.
13. Davies AJ, Rosenwald A, Wright G, et al. Transformation of follicular lymphoma to diffuse large B-cell lymphoma proceeds by distinct oncogenic mechanisms. *Br J Haematol*. 2007;136(2):286-293.
14. Dave SS, Wright G, Tan B, et al. Prediction of survival in follicular lymphoma based on molecular features of tumor-infiltrating immune cells. *N Engl J Med*. 2004;351(21):2159-2169.
15. Wright G, Tan B, Rosenwald A, Hurt EH, Wiestner A, Staudt LM. A gene expression-based method to diagnose clinically distinct subgroups of diffuse large B cell lymphoma. *Proc Natl Acad Sci U S A*. 2003;100(17):9991-9996.